A high temperature dual-mode quartz crystal microbalance technique for erosion and thermal desorption spectroscopy measurements

Reinhard Stadlmayr, Paul Stefan Szabo, Herbert Biber, Hans Rudolf Koslowski, Elisabeth Kadletz, Christian Cupak, Richard Arthur Wilhelm, Michael Schmid, Christian Linsmeier, and Friedrich Aumayr

View Online   **Export Citation**   **CrossMark**

ARTICLES YOU MAY BE INTERESTED IN

A highly sensitive quartz-crystal microbalance for sputtering investigations in slow ion–surface collisions
Review of Scientific Instruments **70**, 3696 (1999); https://doi.org/10.1063/1.1149979

Movable holder for a quartz crystal microbalance for exact growth rates in pulsed laser deposition
Review of Scientific Instruments **91**, 065003 (2020); https://doi.org/10.1063/5.0007643

An ultrahigh vacuum-compatible reaction cell for model catalysis under atmospheric pressure flow conditions
Review of Scientific Instruments **91**, 125101 (2020); https://doi.org/10.1063/5.0026171
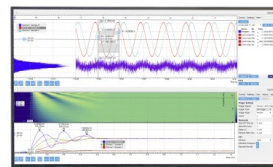
A high temperature dual-mode quartz crystal microbalance technique for erosion and thermal desorption spectroscopy measurements

View Online   Export Citation   CrossMark

Reinhard Stadlmayr,[1,a] (ID) Paul Stefan Szabo,[1] (ID) Herbert Biber,[1] (ID) Hans Rudolf Koslowski,[2] (ID)
Elisabeth Kadletz,[1] (ID) Christian Cupak,[1] (ID) Richard Arthur Wilhelm,[1] (ID) Michael Schmid,[1] (ID)
Christian Linsmeier,[2] (ID) and Friedrich Aumayr[1,a] (ID)

AFFILIATIONS

[1] TU Wien, Institute of Applied Physics, Fusion@ÖAW, 1040 Vienna, Austria
[2] Forschungszentrum Jülich GmbH, Institut für Energie- und Klimaforschung - Plasmaphysik, 52425 Jülich, Germany

[a] Authors to whom correspondence should be addressed: stadlmayr@iap.tuwien.ac.at and aumayr@iap.tuwien.ac.at

ABSTRACT

An improved quartz crystal microbalance measurement method is described, which allows us to determine erosion, implantation, and release rates of thin films, during changing temperatures and up to 700 K. A quasi-simultaneous excitation of two eigenmodes of the quartz resonator is able to compensate for frequency drifts due to temperature changes. The necessary electronics, the controlling behavior, and the dual-mode temperature compensation are described. With this improved technique, quantitative *in situ* temperature-programmed desorption measurements are possible and the quartz crystal microbalance can be used for quantification of thermal desorption spectroscopy measurements with a quadrupole mass spectrometer. This is demonstrated by a study of the retention and release behavior of hydrogen isotopes in fusion-relevant materials. We find that more than 90% of the deuterium implanted into a thin film of beryllium is released during a subsequent temperature ramp up to 500 K.

Published under license by AIP Publishing. https://doi.org/10.1063/5.0012028

I. INTRODUCTION

Quartz crystal microbalance (QCM) layer thickness measurements are based on microweighing by frequency measurements of oscillating crystals, covered with a thin film of a sample material. This technique has a long history and was established by Sauerbrey already in 1959.[1] Based on the piezoelectric effect, a QCM allows measuring mass changes with high accuracy since resonance frequencies can be determined very precisely.[1–4] QCMs have established themselves as a standard method and are widely used in industry to monitor and control coating processes but also for laboratory experiments on film growth via molecular beam epitaxy (MBE)[5,6] or pulsed laser deposition (PLD).[7–9]

The technique can also detect mass losses, which allows us to study in detail the ion-induced erosion and sputtering of surfaces. This is of high interest for investigating plasma–wall interaction processes in nuclear fusion[10–15] but also for studying space weathering effects.[7,16] While QCM measurements are usually performed near room temperature or at somewhat elevated temperatures, e.g., at an extremum of the frequency vs temperature curve of the quartz crystal,[2] higher temperatures can be achieved with temperature compensation,[17] usually limited by the phase transition from α to β quartz at 847 K.[18] Further research showed that it is possible to operate quartz crystals even in the β phase, up to around 1500 K,[19] but with substantially reduced performance due to weaker piezoelectric coupling. Alternatively, the usage of gallium orthophosphate ($GaPO_4$) as a quartz substitute allows operating temperatures up to $\approx$1200 K.[20]

Commercially available high-temperature QCMs usually require a constant operating temperature, which makes them unsuitable for temperature-programmed desorption (TPD) measurements, where continuous changes in operating temperatures are necessary. The objective of this work is to demonstrate the feasibility of a highly sensitive high-temperature QCM, capable of

performing *in situ* TPD measurements, by compensating frequency changes caused by temperature changes, using a dual-mode temperature compensation technique, as presented in a similar way in Refs. 21–23. We have applied this technique up to temperatures of 700 K.

II. BASICS OF THE QCM TECHNIQUE

Sauerbrey developed the fundamentals of the QCM technique. The basis is the fact that the resonance frequency of a quartz crystal depends on the mass of the material deposited on it. The relative change in the resonance frequency $\Delta f/f$ is given by the relative change in the mass $\Delta m/m$,[1]

$$-\frac{\Delta f}{f} = \frac{\Delta m}{m}. \tag{1}$$

Equation (1) holds true for film thicknesses much thinner than the quartz thickness. Typically, coated layers, with a thickness of some 100 nm, are about three orders of magnitude thinner than the quartz itself. Therefore, the initial mass m can be approximated with the quartz mass neglecting the contribution of the coated layer and the different elastic properties (acoustic impedances).[1,24,25]

Changes in the temperature and mechanical stress also cause changes in the resonance frequency of a quartz crystal, which need to be taken into account in order to reach a high sensitivity for mass changes. In fact, quartz sensors can also be used to measure these quantities.[3,21,26,27]

Equation (1) can be extended to evaluate mass change rates, by considering the time derivative of the frequency, as can be seen in the following equation:

$$\frac{\Delta m}{\Delta t} = -\frac{m_0}{f_0}\frac{\Delta f}{\Delta t}, \tag{2}$$

where f_0 and m_0 represent the initial resonance frequency and the initial mass of the quartz crystal. A QCM allows *in situ* measurements of mass changes; therefore, this form of representation is more suitable.

In order to evaluate sputtering yields by particle irradiation, beam parameters can be included in Eq. (2). This is done by considering the target particle mass m_T, projectile flux density Φ, and surface area of the quartz sample A_q, by which the sputtering yield Y (removed atoms per incoming ion) can be determined according to Eq. (3).[2,10] In order to avoid an influence by the non-uniform radial sensitivity[3,28] of the quartz disc, it is necessary to distribute the projectile flux evenly over the active area of the quartz sample,[2,10]

$$Y\,(\text{atoms/ion}) = \frac{1}{\Phi\,A_q\,m_T}\frac{m_0}{f_0}\frac{\Delta f}{\Delta t}. \tag{3}$$

III. QCM ELECTRONICS

The QCM electronics used in the present work were originally developed at TU Wien and are described in detail by Hayderer *et al.*[2] The setup measures the resonance frequency of a quartz crystal, which oscillates at 6 MHz, with an precision in the mHz range. When the quartz crystal temperature is stabilized at an extremum of the frequency vs temperature curve of the quartz

crystal, the precision is limited by the crystal resonance frequency drift of about 2 mHz/min and the noise of the electronics of about 5 mHz. This allows us to detect mass changes in the order of 10 pg cm^{-2} s^{-1}, which is equivalent to a tungsten erosion rate of about 10^{-4} W monolayers/s or an deuterium outgassing rate of about 3×10^{12} D cm^{-2} s^{-1}.[2,10]

Applying the QCM to sputtering, where implanted ions and radiation damage lead to large stress in the film, demands the use of stress compensated (SC-cut) quartz crystals. This quartz type has a lower sensitivity to thermal and mechanical stress, compared to the most commonly used AT-cut quartz crystals.[2,3] Our QCM uses plano-convex SC-cut quartz crystal resonator discs (14 mm diameter) with the product specification XA-3641 from the company KVG Quartz Crystal Technology GmbH. A thickness of 0.30 mm and a radius of curvature of 300 mm lead to a fundamental-mode frequency of 6 MHz.

Figure 1 shows the schematics of the QCM electronics, which are used for driving the quartz crystal at its resonance frequency. The quartz crystal is operated in series resonance, either at its fundamental mode (C1 mode) at 6 MHz or in the C3 overtone mode at around 18 MHz. The so-called phase box includes the main parts of the driving electronics and is located outside the ultra-high vacuum (UHV) chamber. This part of the electronics is identical to that of Ref. 2. Electrical feedthroughs in combination with UHV coaxial cables (coax) connect the quartz crystal to the phase box. A sine wave is generated by using a personal computer (PC)-controlled function generator (Tektronix AFG2021) and is fed into the phase box. The function generator uses a 10 MHz oven-controlled crystal oscillator (OCXO) reference frequency (IQD IQOV-164-4) with a short term stability (Allan variance) of 0.01 ppb/s to ensure high precision. The electric circuit in the phase box provides a signal that depends on the deviation of the input frequency from the series resonance frequency of the quartz crystal, by using a phase comparison technique between the current and voltage. An automated gain control with a voltage controlled amplifier (VCA) ensures a constant current through the quartz crystal. A differential setup with a separate and open ended coax cable, which has exactly the same length as the one connected to the quartz crystal, compensates for the cable capacity. At resonance, the phase shift between the voltage and current is zero, which leads to a zero voltage at the frequency control output. In any other case, a positive or negative voltage can be measured at the frequency control output, meaning that the actual supplied frequency is too high or too low. More details on the phase box design can be found in Ref. 2 (the circuit diagram and component list of the phase box are available from the authors upon request). The frequency control output voltage is fed into a fast analog-digital-converter (ADC) (National Instruments USB-6210), connected to a PC. A controlling script written in Python adjusts the function generator's output frequency.

Hayderer *et al.* used a voltage-controlled oscillator for feeding the sine wave voltage to the phase box. The actual resonance frequency was then measured by using a frequency counter.[2] This resulted in a bulky setup. By replacing both devices with one high-precision PC-controlled function generator and a compact ADC, the size of the whole QCM electronics was substantially reduced. The function generator can be set by a digital interface, making an additional frequency counter obsolete. Furthermore, the operational frequency range is not limited to 5.9 MHz–6.1 MHz anymore,
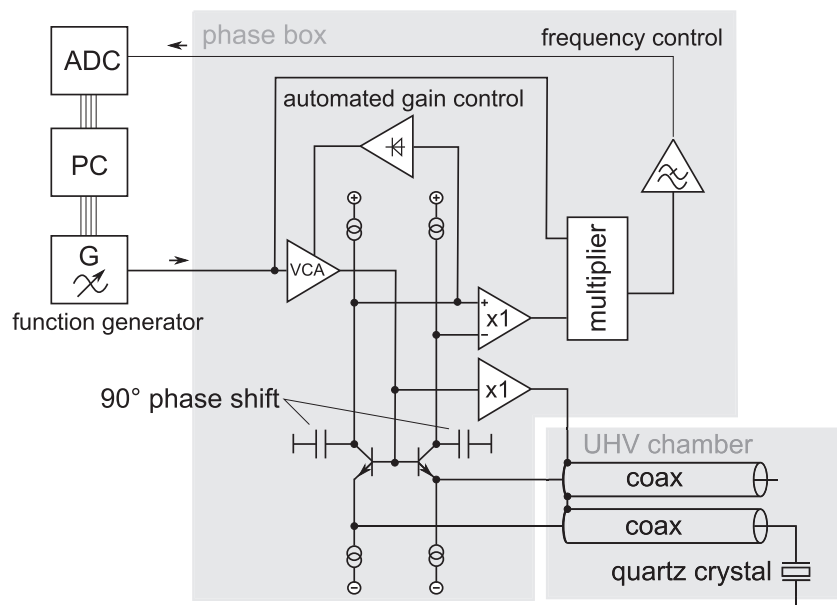
FIG. 1. QCM electronic schematics. The so-called phase box measures the phase of the admittance of the quartz crystal and provides it as an analog signal at the frequency control output. In the present setup, this output is read via an ADC, which is connected to a PC. A controlling script on this PC then adjusts the function generator output frequency to keep the quartz crystal in resonance. Adapted with permission from Hayderer *et al.*, Rev. Sci. Instrum. **70**, 3696 (1999). Copyright 1999 AIP Publishing LLC.

allowing for the first time operation of the TU Wien QCM in the overtone mode up to 20 MHz. The use of a PC as a controlling device also allows us to rapidly switch between resonance frequencies and enables a quasi-simultaneous operation of two or more frequency modes.

IV. DUAL-MODE TECHNIQUE

The new digitalized QCM electronic setup allows us to excite any quartz crystal modes up to 20 MHz. Only the main C-modes are of interest because for SC-cut crystals, they are insensitive to radial stress. Furthermore, the C1 and C3 modes are well separated from the side-resonances of the A and B modes, so unwanted mode coupling does not occur.[3,4] The C1 main mode is the resonance frequency used in the conventional single-mode technique, as described in Ref. 2. Due to the large frequency range of the function generator, care must be taken not to excite any secondary modes of the quartz crystal, which have a different sensitivity to mass and temperature changes. Except for extremely thick films, only odd overtone modes are excitable;[28] therefore, the second mode of interest is the C3 mode.[3,4] The C1 and C3 modes have a linear dependence on mass changes but a different response to changes in temperature. Measuring the frequencies of both modes makes it possible to eliminate temperature effects from the data.[21]

A. Principle of dual-mode controlling

The improved QCM technique quasi-simultaneously excites the fundamental mode (C1 mode) and the third overtone mode (C3 mode) of a quartz crystal sample. Every 5 s, a proportional-integral-derivative (PID) software controller switches the sine wave frequency generator's output between both frequencies, where the PID controlling parameters were optimized for both modes. The time constants of the controller for the C1 and C3 modes can be

found in Table I. (We do not provide the proportional gains since they depend on the details of the implementation, such as the gain of the phase-to-voltage conversion. The proportional gains required for the C1 and C3 modes are essentially identical.) We have used a controller cycle time of $\Delta t = 50$ ms. The resonance frequency recorded is the final frequency after switching to the C1 or C3 mode and running the PID controller for 5 s.

The fundamental mode frequency can be measured up to a precision in the mHz range, while the third overtone mode is limited to about 100 mHz due to increased noise and signal damping in the electronics at this frequency.

The frequency control output of the phase box provides a signal that is in first order proportional to the deviation from the resonance frequency and allows the controller to lock onto the resonance frequency (as described in Sec. III) but only in a small frequency range. Due to the strong response of the feedback voltage at resonance, the C1 mode can be found rather easily. Here, the phase box and the controller are able to find the precise resonance frequency over a starting frequency range of $\Delta f \approx 100$ kHz.[2]

In contrast, it is more difficult to find the C3 mode frequency because the resonance response is less pronounced. Compared to the C1 mode, the motional capacitance of the third overtone is reduced by a factor of $1/9$ due to the overtone number and another factor of $\approx 1/3$ due to the lower active area.[3,28]

TABLE I. PID controlling parameters for the fundamental mode C1 and overtone mode C3.

PID controlling parameters	C1 (s)	C3 (s)
Integration time T_i	1.25	3
Derivative time T_d	0.06	0.6

Furthermore, the risk of exciting secondary modes is high.[3,4,29] The frequency range for locking to the C3 mode is smaller and only in the range of about $\Delta f \approx 20$ kHz. This means the position of the frequency of the third mode needs to be preset as well as possible before the start of the dual-mode QCM operating.

Due to the plano-convex geometry of the used quartz crystal, the C3 mode frequency is lower than three times the C1 mode frequency.[30,31] Experiments have revealed a simple rule of thumb to find this frequency position.

For the crystals used, we can estimate the frequency f_3 of the C3 mode from that of the fundamental C1 mode (f_1), as described in the following equation:

$$f_3 \approx 3f_1 - 1.6 \times 10^5 \text{ Hz}. \tag{4}$$

This approximation is accurate within a range of 20 kHz, which is good enough for the QCM controller to lock on the precise resonance frequency.

It should be noted that the C3 mode frequency is below three times the C1 mode frequency, which provides an upper limit for the controller and avoids exciting unwanted secondary modes as well as B-mode resonance frequencies, which lie above C-mode frequencies.[4] As soon as the two resonance frequencies f_1 and f_3 have been found, when switching between the two resonances, the controller always uses the previously determined frequency value of the given mode as the starting point.

B. Dual-mode temperature compensation

The resonance frequency of a quartz crystal is very sensitive to changes in temperature, which causes difficulties in separating the change in the resonance frequency due to mass change and temperature change. A common way is to operate the quartz crystal in its fundamental mode at an elevated temperature where its frequency exhibits a minimum (see the green curve in Fig. 2). Here, temperature changes of a few K cause only small changes in the resonance frequency.[2,10,14]

In order to perform temperature-programmed desorption (TPD) measurements with a QCM, the change in resonance frequency due to temperature change needs to be taken into account.
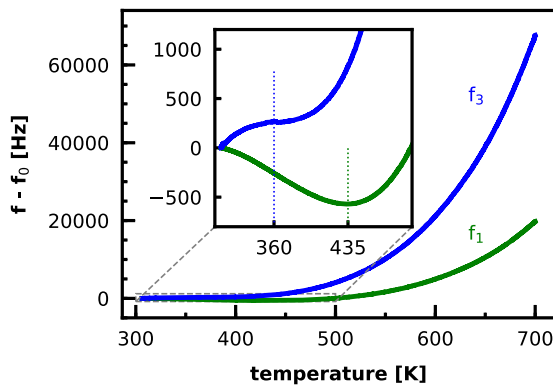
FIG. 2. Temperature responses of the C1 fundamental mode f_1 and C3 overtone mode f_3 of a Be-coated quartz crystal sample, without changes in mass. The 300 K–500 K range is enlarged in the inset.
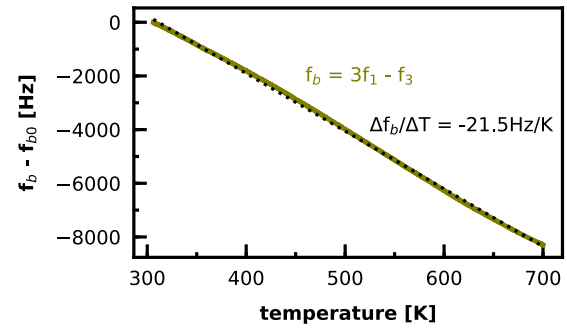
FIG. 3. The beat frequency f_b of a Be-coated quartz crystal sample, measured from room temperature to 700 K. A nearly linear behavior can be seen. The dotted line shows a linear fit with a slope of $\Delta f_b/\Delta T = -21.5$ Hz/K.

The C1 and C3 modes of a quartz crystal have a linear dependence on mass changes (as can be seen in Sec. VI A) but a different response to changes in temperature.

Figure 2 shows the temperature dependence of the C1 mode (f_1) and the C3 mode (f_3) of an SC-cut quartz crystal. The C3 mode shows a saddle point at 360 K, while the C1 mode has a local minimum at 435 K. Further increasing the temperature leads to a strong increase in both resonance frequencies.

By defining a beat frequency f_b [Eq. (5)], a nearly linear dependence of f_b on the real temperature can be seen, as proposed by Pierce et al,[21]

$$f_b = 3f_1 - f_3. \tag{5}$$

The result of a test measurement is shown in Fig. 3, where a Be-coated quartz crystal was heated up to 700 K and f_b evaluated. Due to its almost linear temperature dependence, f_b can be used as a quartz internal thermometer.[21] In order to perform the temperature compensation, the Sauerbrey equation (1) needs to be extended to also include the temperature (T), as can be seen in the following equations:

$$\frac{\Delta f_1(m, T)}{f_{10}} = \frac{\Delta f_1(m)}{f_{10}} + \frac{\Delta f_1(T)}{f_{10}} = -\frac{\Delta m}{m_0} + \frac{\Delta f_1(T)}{f_{10}} \tag{6}$$

and

$$\frac{\Delta f_3(m, T)}{f_{30}} = -\frac{\Delta m}{m_0} + \frac{\Delta f_3(T)}{f_{30}}. \tag{7}$$

This extension includes both modes and the temperature dependence (index 1 for the fundamental mode and index 3 for the third overtone mode, where "10" and "30" denote the initial frequencies at 300 K).

Due to the nearly linear temperature dependence of the beat frequency, and as it does not depend on the mass change Δm, f_b can be used as a temperature gauge. In order to calibrate the temperature-induced frequency vs beat frequency, a frequency vs temperature measurement was conducted, without any mass change. The result is shown in Fig. 2. A polynomial of fifth order was used to fit this separate measurement for both eigenfrequencies, according to the following equations, as this order is sufficient for

the residuals being dominated by the experimental scatter and not by the fit function:

$$f_1(T) \Rightarrow f_1(f_b) = \sum_{i=0}^{5} a_i \times (f_b)^i, \tag{8}$$

$$f_3(T) \Rightarrow f_3(f_b) = \sum_{i=0}^{5} b_i \times (f_b)^i. \tag{9}$$

Combining Eqs. (6)–(9) and the conversion to mass change rate finally lead to a temperature-compensated mass change rate,

$$\frac{\Delta m}{\Delta t} \text{ (amu/s)} = -\frac{m_0}{2} \left[\frac{1}{f_{10}} \left(\frac{\Delta f_1}{\Delta t} - \frac{\Delta f_1(f_b)}{\Delta t} \right) + \frac{1}{f_{30}} \left(\frac{\Delta f_3}{\Delta t} - \frac{\Delta f_3(f_b)}{\Delta t} \right) \right]. \tag{10}$$

In principle, a temperature compensated mass change rate can also be realized by combining only Eqs. (6) and (8) or only Eqs. (7) and (9), but the numerical accuracy is increased by taking an average over both modes, as can be seen in Eq. (10).

Absolute temperature measurements of a quartz crystal, e.g., with a thermocouple (TC), are disadvantageous, as the temperature cannot be measured directly on the quartz crystal but only on the sample holder. This would cause a shift between the real temperature of the quartz sample and the temperature measured via TC. The beat frequency, instead, is directly related to the temperature of the quartz crystal and gives a more reliable temperature information. As soon as the relation between the beat frequency and the temperature is known for the given crystal, this dual-mode technique makes measurements of the temperature with an external device obsolete during measurements of the sputtering yield or desorption. The absolute value can be obtained from calibration at room temperature, where the sample holder and quartz are both at the same temperature.

V. IRRADIATION SETUP

Erosion and implantation measurements were performed under UHV conditions, with a base pressure of about 10^{-9} mbar. A sputter ion source (Specs IQE 12/38 and Prevac IS40E1) was used to provide an ion beam with energies from $E_{kin} = 100$ eV to 5 keV and a D flux density of up to $\Phi \approx 10^{18}$ m^{-2} s^{-1}.

Figure 4 shows the 3D computer aided design (CAD) drawing of the used quartz sample holder.[32] It is separated in two sections: The upper part consists of a Faraday cup with a secondary electron suppressor, for an accurate determination of the ion flux. The lower part includes the quartz crystal and a resistive heating system used to operate the crystal at elevated temperatures and for TPD measurements. A K-type TC, mounted laterally on the sample holder, is used for measuring the temperature.

A. Measurement procedure

By using a Faraday cup, embedded in the sample holder with the quartz crystal, the ion flux Φ is measured. The beam profile is obtained by lateral displacement of the sample holder in the y and z direction in mm steps. The ion beam is adjusted so that the variations of the ion current density are less than 10% over the scanning
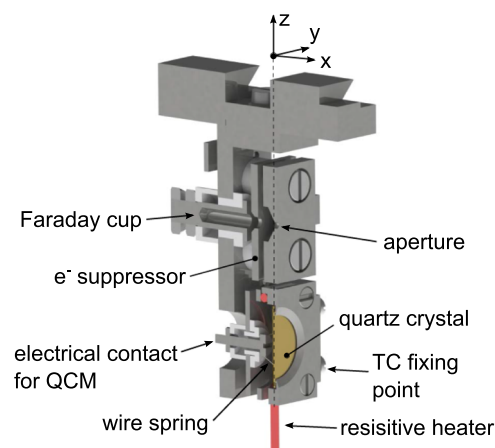

FIG. 4. Sectional drawing of the QCM sample holder. It is separated in two sections, which can be moved into the ion beam, by linear movement of the sample holder in the z direction: (top) a Faraday cup with a secondary electron suppressor and aperture for ion beam analysis; (bottom) the quartz holder including the quartz crystal disc with a diameter of 14 mm and a resistive heater equipment. A K-type TC is mounted on one side of the holder. The dashed line indicates the rotation axis, which runs exactly through the center of the quartz crystal as well as the aperture of the Faraday cup.

range of 5 × 5 mm^2. After successful adjustment of the ion beam, the quartz crystal is moved into the ion beam and the frequency change is recorded. Since no measurement of the ion beam is possible during irradiation of the sample, the ion beam flux is checked before and after every irradiation step. For sputtering yield evaluation according to Eq. (3), both ion flux measurements are averaged. Deviations caused by the non-uniform ion beam and between both ion flux measurements are taken into account for the determination of the error bars.

VI. RESULTS

A. System verification by Ar on Au erosion measurements

A measurement was carried out by irradiating an Au-coated quartz sample at room temperature to verify the expected C3 overtone mode behavior under ion-induced erosion. The Au coating, fabricated via sputter deposition at the Institute of Solid State Physics at TU Wien, had a thickness of 500 nm. Figure 5 shows the results of this dual-mode QCM sputtering yield measurement, where an Ar$^+$ ion beam with an energy of $E_{kin} = 500$ eV hits an Au-coated quartz sample under normal incidence and at room temperature (300 K). During the beam-on phase ($t = 200$ s–800 s), a constant increase in the resonance frequency can be seen, which is equivalent to a mass loss. By evaluating the ion flux density Φ, as described in Sec. II, the sputtering yield Y can be calculated.

Using the fundamental mode leads to a sputtering yield of $Y_{Ar \to Au, C1} = 2.72 \pm 0.18$, and by using the third overtone mode, a sputtering yield of $Y_{Ar \to Au, C3} = 2.70 \pm 0.17$ can be measured. Both modes provide very similar sputtering yields, but absolute changes in the resonance frequency are three times higher while using the third
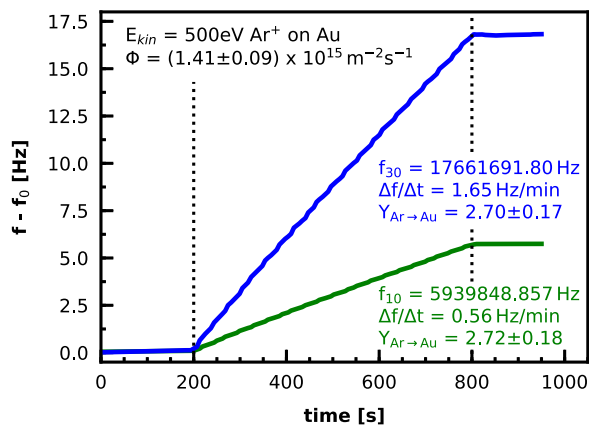
FIG. 5. Ar^+ on the Au sputtering yield measurement, showing the QCM frequency response over time of the fundamental (C1) mode (green) and the third overtone (C3) mode (blue). During the beam-on phase between $t = 200$ s and $t = 800$ s, an Ar^+ ion beam with 500 eV hits the Au-coated quartz sample under normal incidence, where a continuous increase in the resonance frequencies can be seen. The slopes $\Delta f/\Delta t$ during the beam-on phase and the ion beam flux Φ were used to evaluate the sputtering yields Y. Small wiggles in the signal are caused by the controller switching between the modes.

FIG. 6. Fluence dependence of the fundamental-mode resonance frequency of the quartz crystal sample (blue) and the mass change rate (Δm rate) (green) of a Be sample under D irradiation with 2.5 keV and normal incidence. The implantation of D can be seen as a decrease in the resonance frequency as well as a positive Δm rate (β_1 and β_2 regions). The saturation of the sample occurs after a fluence of 6.7×10^{21} m^{-2}, whereupon sputtering takes over as the dominant process (γ region). The beam switch-on (α) and beam switch-off (Ω) regions are equivalent in height of about 12 Hz.

overtone mode. This result confirms that the Sauerbrey equation (1) holds true for the C3 overtone mode.

B. Retention and release of D in Be

For deuterium implantation and TPD measurements, Be-coated quartz crystals were used. These coatings were fabricated by using a thermionic vacuum arc (TVA) technique at the National Institute of Laser, Plasma and Radiation Physics in Bucharest.[33] 500 nm thick Be films were deposited on top of an electrode of the quartz crystals. Before deuterium implantation, the surface was sputter-cleaned of possible oxides with an Ar ion beam at an angle of incidence of $60°$.

1. D implantation in Be

Implantation was performed at room temperature (300 K) and under normal incidence of the D_2^+ ions, up to a fluence of $(9.9 \pm 0.6) \times 10^{21}$ m^{-2}. Since the sputter ion source delivers the highest ion current by using D_2^+ ions, this projectile was used for implantation, where the kinetic energy of 5 keV per D_2 is equivalent to 2.5 keV per D. This factor of 2 is also considered in the determination of the ion flux, where we assume that a D_2^+ ion flux corresponds to twice as the high D^+ ion flux. In our case, an average D ion flux of $\Phi = (7.9 \pm 0.5) \times 10^{17}$ m^{-2} s^{-1} could be reached. At this kinetic energy of 2.5 keV per D, an implantation depth of about 70 nm can be expected, according to binary collision approximation (BCA) codes, like SRIM or SDTrimSP.[34,35] In Fig. 6, the results of the implantation measurement of D in Be are shown. As the trend is very similar, only the fundamental-mode frequency f_1 is shown.

The QCM technique allows highly accurate mass change measurements, but only determination of the net mass change is possible.[2] During ion bombardment of a sample, implantation as well as sputtering and outgassing occurs. The implantation-dominated
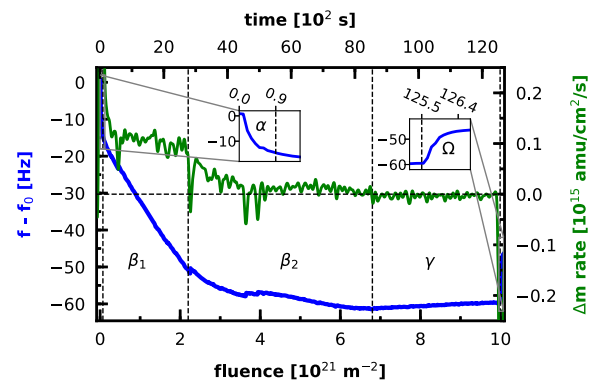
regime can be seen as a drop in the resonance frequency of the crystal, which is equivalent to a positive mass change rate and, therefore, an increase in the sample mass. As soon as saturation occurs, the mass change rate becomes negative, meaning that sputtering overtakes as the dominant process.

The implantation measurement shows different regions, which can be interpreted as follows (compare with Fig. 6):

α—switch-on region: The frequency change is larger than what could be explained by implantation. Therefore, it is dominated by thermal stress due to a slight temperature increase in the central region of the crystal, caused by the energy deposited by the ions. In the measurement, a fast frequency drop of 12 Hz can be seen, and after a fluence of about 7×10^{19} m^{-2}, the linear implantation region starts.

β—implantation region: Here, the quartz crystal is in thermal and stress equilibrium and the implantation of projectiles continues, showing a positive and constant mass change rate of about 1.1×10^{14} amu cm^{-2} s^{-1}, as well as a continuous decrease in the resonance frequency. Defects in amorphous Be are filled up, in combination with chemical bonding to Be as well as impurities,[36] which can be seen in a high mass change rate (β_1 region). After a fluence of about 2.2×10^{21} m^{-2}, the mass change rate decreases, showing that easily accessible defects in the sample are nearly filled up (β_2 region).

γ—sputtering region: After a fluence of 6.7×10^{21} m^{-2}, the sample is saturated and the mass change rate (Δm rate) becomes slightly negative, which means that sputtering overtakes as the dominant process. By evaluating the slope of the frequency response in this region, a sputtering yield of $Y_{D \to Be} = 0.005$ Be/D can be obtained.

Ω—switch-off region: After a fluence of 9.9×10^{21} m^{-2}, the ion beam is switched off. The frequency change is due to the release of the thermal stress on the quartz crystal, as the ion beam is switched off and no energy is deposited any more as well as, possibly, due

to desorption of shallow implants diffusing to the surface. As the frequency changes in the α and Ω regions are comparable but of opposite sign (compare the two insets in Fig. 6), the main contribution to these changes must be attributed to thermal stress. After switching off the ion beam, no more fluence is applied. Therefore, the abscissa in the insets of Fig. 6 is given in time units, not fluence units.

The measured mass change rate also allows us to determine the total mass change during this irradiation by integration. Here, a total mass increase of $\Delta m = 381 \times 10^{15}$ amu/cm^2 could be evaluated. As the QCM technique allows us to measure the total mass change only, sputtering needs to be considered. By considering a sputtering yield of $Y_{D \to Be} = 0.005$ Be/D, as evaluated from the γ region, which corresponds to a loss of Be and is compensated by implantation of D, the total implanted mass raises to $\Delta m = 425 \times 10^{15}$ amu/cm^2.

In the current work as well as in Ref. 2, we employ SC-cut quartz crystals. The resonance frequency of this particular crystal orientation is insensitive to isotropic in-plane stress, as it occurs due to ion implantation.[37,38] This is especially important if the thickness affected by the ion beam is larger than that of the material added or removed, which is the case for the measurements presented in Fig. 6, while its impact on deposition measurements is rather limited.[9] Since the stress sensitivity of the resonance frequency depends on the azimuthal orientation of the stress and both the heat conductivity and thermal expansion of quartz are anisotropic, the SC-cut is not perfectly compensated for thermal stress caused by heating the center of the crystal (in the present case, caused by the energy deposited by the impinging ions and the edge of the crystal kept at a lower temperature). This effect can be seen in Fig. 6.

2. TPD measurements

After implantation, a TPD measurement was initiated. The resistive heater wires of the sample holder in combination with a computer-controlled current supply and an attached TC (compare with Sec. V) were used to perform a heating ramp with a rate of
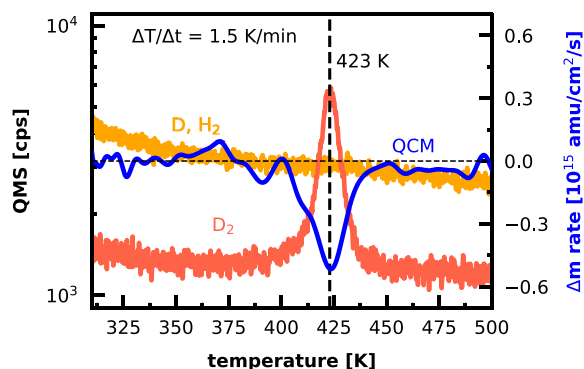
FIG. 7. TPD result after D implantation in Be. The QMS revealed a pronounced D$_2$ outgassing, peaking at 423 K with a QMS count rate of 6×10^3 cps. The QCM confirms this peak, showing a negative peak of the mass change rate. By integrating over this peak, a total mass loss of $\Delta m = -394 \cdot 10^{15}$ amu/cm^2 can be evaluated.

TABLE II. Comparison of the total applied fluence to the measured mass change (Δm) during the implantation of D$_2$ in Be and subsequent TPD. The percentages refer to the total applied fluence. The mass loss measured with the QCM (using dual-mode temperature compensation) during TPD is lower compared to the mass increase caused by implantation.

Total applied fluence	9.9×10^{21} D/m^2 = 1980×10^{15} amu/cm^2	
Δm implantation	$+425 \times 10^{15}$ amu/cm^2	21.5%
Δm TPD ($m = 4$ peak)	-394×10^{15} amu/cm^2	19.9%

1.5 K/min. A quadrupole mass spectrometer (QMS) attached to the chamber, with a distance of about 10 cm of the sensor head to the sample, was used to analyze the outgassing elements and molecules.

In Fig. 7, the TPD results can be seen, from room temperature to 500 K. The QMS signal shows a pronounced $m/q = 4$ (D$_2$) peak at a temperature of 423 K, while in the $m/q = 2$ signal (H$_2$ and D), only a continuous decrease in the signal can be seen. The blue line in this signal shows the resulting mass change rate evaluated simultaneously via the dual-mode QCM technique. It confirms a negative mass change, peaking at 423 K and, thus, clearly displays the outgassing of D, which desorbs as D$_2$. By integrating the mass change rate over this peak, a total mass loss of $\Delta m = -394 \cdot 10^{15}$ amu/cm^2 could be quantitatively evaluated.

In Table II, the mass change rates evaluated during implantation and during the TPD are compared to the total applied fluence. During implantation, 21.5% of the total applied D fluence was implanted into the sample, while during the TPD, a value of 19.9% was emitted. Although an error in the total applied fluence of about 6% needs to be considered here, it is noteworthy that about 93% of the implanted D is released during the TPD temperature ramp up to 500 K.

VII. SUMMARY AND CONCLUSION

An improvement of the TU Wien QCM technique was presented, which allows us to operate a quartz crystal sample in overtone modes. A quasi-simultaneous excitation of the fundamental mode (C1) and the third overtone mode (C3) of a quartz crystal allows us to compensate for frequency changes caused by temperature changes. This principle is based on an idea from Refs. 21–23. We were able to show that this technique can be used to perform high-temperature QCM measurements up to 700 K.

The QCM electronics described in Ref. 2 were modified by using a software-controlled high-precision function generator, which extends the driving frequency range up to 20 MHz. This maximum frequency is limited by the function generator used but could be further increased by using a different generator. However, care must be taken that the performance of the current phase-detection electronics becomes less satisfactory at high frequencies, and at the same time, the admittance change in the quartz crystal at the resonance also decreases with overtone number, which makes it more difficult to lock on the resonance frequencies with higher

precision. Furthermore, the broad frequency range increases the risk of exciting unwanted side-mode resonances.

The quasi-simultaneous excitation of two eigenmodes by switching between the frequencies is advantageous, as the driving electronics only have to be designed once. Furthermore, the interference by simultaneous excitation of several resonances is intrinsically avoided. It was shown that erosion rates can also be evaluated with the C3 mode.

This technique was used for the first time to investigate the implantation and release behavior of D in Be. A total D fluence of 9.9×10^{21} m^{-2} was applied, where the QCM mass change measurements during implantation showed that 21.5% of the applied D fluence was implanted. A subsequent TPD measurement in combination with the new QCM dual-mode temperature compensation technique revealed a total mass release of 20% of the total applied D fluence. This means that over 90% of the implanted D is again released during the temperature scan up to 500 K, with a pronounced release peak of D observed very clearly at a temperature of 423 K.

Oberkofler et al.[39] found out that a threshold fluence needs to be implanted first in order to see this "low-temperature" release peak at all, whereon the maximum of this peak shifts to lower temperatures at higher fluences. Furthermore, they found out that between 700 K and 850 K, further D is released. This was also confirmed by Eichler.[40]

Since in a future fusion facility, such as ITER, temperatures around 900 K are expected for a Be blanket plasma-facing-component, the fusion fuel implanted in the wall will immediately outgas, and therefore, the retention will be low.[41–44]

Unfortunately, this temperature range is not accessible with our current QCM technique. As mentioned above, beyond 846 K, the stable phase of quartz is the β phase, and returning to the α phase at lower temperatures would make the quartz crystals essentially unusable due to twinning. Even if the β phase is piezoelectric, its low coupling constant would make excitation of the third harmonic overtone very difficult. Furthermore, it is unclear whether this particular crystal orientation is still stress-compensated in the β phase. A better alternative for high-temperature measurements would be the use of gallium orthophosphate (GaPO$_4$) crystals, which are stable up to 1200 K and also provide stronger piezoelectric coupling than SiO$_2$.[20]

ACKNOWLEDGMENTS

DATA AVAILABILITY

The data that support the findings of this study are available from the corresponding author upon reasonable request.

REFERENCES

[1] G. Sauerbrey, Z. Phys. **155**, 206 (1959).

[2] G. Hayderer, M. Schmid, P. Varga, H. Winter, and F. Aumayr, Rev. Sci. Instrum. **70**, 3696 (1999).

[3] E. Benes, M. Gröschl, W. Burger, and M. Schmid, Sens. Actuators, A **48**, 1 (1995).

[4] M. Schmid, "Möglichkeiten und grenzen der schwingquarz-schichtdickenmessung," Ph.D. thesis, TU Wien, 1989.

[5] D. S. Katzer, N. Nepal, D. J. Meyer, B. P. Downey, V. D. Wheeler, D. F. Storm, and M. T. Hardy, Appl. Phys. Express **8**, 085501 (2015).

[6] C. D. Theis and D. G. Schlom, J. Cryst. Growth **174**, 473 (1997).

[7] P. Szabo, R. Chiba, H. Biber, R. Stadlmayr, B. M. Berger, D. Mayer, A. Mutzke, M. Doppler, M. Sauer, J. Appenroth, J. Fleig, A. Foelske-Schmitz, H. Hutter, K. Mezger, H. Lammer, A. Galli, P. Wurz, and F. Aumayr, Icarus **314**, 98 (2018).

[8] A. A. Voevodin and S. J. P. Laube, Surf. Coat. Technol. **76-77**, 670 (1995).

[9] G. Franceschi, M. Schmid, U. Diebold, and M. Riva, Rev. Sci. Instrum. **91**, 065003 (2020).

[10] A. Golczewski, K. Dobes, G. Wachter, M. Schmid, and F. Aumayr, Nucl. Instrum. Methods Phys. Res., Sect. B **267**, 695 (2009).

[11] R. Stadlmayr, P. S. Szabo, B. M. Berger, C. Cupak, R. Chiba, D. Blöch, D. Mayer, B. Stechauner, M. Sauer, A. Foelske-Schmitz, M. Oberkofler, T. Schwarz-Selinger, A. Mutzke, and F. Aumayr, Nucl. Instrum. Methods Phys. Res., Sect. B **430**, 42 (2018).

[12] R. Stadlmayr, P. S. Szabo, D. Mayer, C. Cupak, T. Dittmar, L. Bischoff, S. Möller, M. Rasiński, R. A. Wilhelm, W. Möller, and F. Aumayr, J. Nucl. Mater. **532**, 152019 (2020).

[13] R. Stadlmayr, P. S. Szabo, D. Mayer, C. Cupak, W. Möller, and F. Aumayr, Phys. Scr. **T171**, 014021 (2020).

[14] B. M. Berger, R. Stadlmayr, D. Blöch, E. Gruber, K. Sugiyama, T. Schwarz-Selinger, and F. Aumayr, Nucl. Mater. Energy **12**, 468 (2017).

[15] K. Dobes, M. Köppen, M. Oberkofler, C. P. Lungu, C. Porosnicu, T. Höschen, G. Meisl, C. Linsmeier, and F. Aumayr, Nucl. Instrum. Methods Phys. Res., Sect. B **340**, 34 (2014).

[16] P. S. Szabo, H. Biber, N. Jäggi, M. Brenner, D. Weichselbaum, A. Niggas, R. Stadlmayr, D. Primetzhofer, A. Nenning, A. Mutzke, M. Sauer, J. Fleig, A. Foelske-Schmitz, K. Mezger, H. Lammer, A. Galli, P. Wurz, and F. Aumayr, Astrophys. J. **891**, 100 (2020).

[17] V. M. Mecea, J. O. Carlsson, P. Heszler, and M. Bârtan, Vacuum **46**, 691 (1995).

[18] R. S. Coe and M. S. Paterson, J. Geophys. Res. **74**, 4921, https://doi.org/10.1029/jb074i020p04921 (1969).

[19] T. Uno, H. Tashiro, and S. Noge, IEEJ Trans. Electron., Inf., Syst. **131**, 1150 (2011).

[20] H. Thanner, P. W. Krempl, W. Wallnöfer, and P. M. Worsch, Vacuum **67**, 687 (2002).

[21] D. E. Pierce, Y. Kim, and J. R. Vig, IEEE Trans. Ultrason., Ferroelectr., Freq. Control **45**, 1238 (1998).

[22] S. S. Schodowski, in Proceedings of the 43rd Annual Symposium on Frequency Control (IEEE, 1989), pp. 2–7.

[23] A. Benjaminson and S. C. Stallings, in Proceedings of the 43rd Annual Symposium on Frequency Control (IEEE, 1989), pp. 20–26.

[24] E. Benes, J. Appl. Phys. **56**, 608 (1984).

[25] C. S. Lu and O. Lewis, J. Appl. Phys. **43**, 4385 (1972).

[26] F. J. Azcondo and J. Peire, in Proceedings IECON '91: 1991 International Conference on Industrial Electronics, Control and Instrumentation (IEEE, 1991), Vol. 3, pp. 2580–2585.

[27] R. J. Besson, J. J. Boy, B. Glotin, Y. Jinzaki, B. Sinha, and M. Valdois, IEEE Trans. Ultrason., Ferroelectr., Freq. Control **40**, 584 (1993).

[28] M. Schmid, E. Benes, W. Burger, and V. Kravchenko, IEEE Trans. Ultrason., Ferroelectr., Freq. Control **38**, 199 (1991).

[29] M. Küstner, W. Eckstein, E. Hechtl, and J. Roth, J. Nucl. Mater. **265**, 22 (1999).

[30] D. S. Stevens and H. F. Tiersten, J. Acoust. Soc. Am. **79**, 1811 (1986).

[31] E. Benes, M. Schmid, and V. Kravchenko, J. Acoust. Soc. Am. **90**, 700 (1991).

[32] B. M. Berger, "Laboratory work on plasma-wall-interaction processes relevant for fusion experiments," Ph.D. thesis, TU Wien, 2017.

[33] C. P. Lungu, I. Mustata, V. Zaroschi, A. M. Lungu, A. Anghel, P. Chiru, M. Rubel, P. Coad, and G. F. Matthews, Phys. Scr. **T128**, 157 (2007).

[34] J. F. Ziegler, M. D. Ziegler, and J. P. Biersack, Nucl. Instrum. Methods Phys. Res., Sect. B **268**, 1818 (2010).

[35] A. Mutzke, R. Schneider, W. Eckstein, R. Dohmen, K. Schmid, U. von Toussaint, and G. Badelow, IPP Report 2019-02, 2019.

[36] K. Sugiyama, C. Porosnicu, W. Jacob, I. Jepu, and C. P. Lungu, Nucl. Mater. Energy **6**, 1 (2016).

[37] E. P. EerNisse, in *29th Annual Symposium on Frequency Control* (IEEE, 1975), pp. 1–4.

[38] E. P. EerNisse, in *30th Annual Symposium on Frequency Control* (IEEE, 1976), pp. 8–11.

[39] M. Oberkofler, M. Reinelt, A. Allouche, S. Lindig, and C. Linsmeier, Phys. Scr. **T138**, 014036 (2009).

[40] M. Eichler, Nucl. Mater. Energy **19**, 440 (2019).

[41] P. Vladimirov, D. Bachurin, V. Borodin, V. Chakin, M. Ganchenkova, A. Fedorov, M. Klimenkov, I. Kupriyanov, A. Moeslang, M. Nakamichi, T. Shibayama, S. V. Til, and M. Zmitko, Fusion Sci. Technol. **66**, 28 (2014).

[42] *Fusion Physics*, edited by M. Kikuchi, K. Lackner, and T. Minh Quang (International Atomic Energy Agency, 2012).

[43] G. Janeschitz, J. Nucl. Mater. **290-293**, 1 (2001).

[44] V. Barabash, G. Federici, R. Matera, A. R. Raffray, and I. Home Teams, Phys. Scr. **T81**, 74 (1999).